

Report

Increased Cell Bond Tension Governs Cell Sorting at the *Drosophila* Anteroposterior Compartment Boundary

Katharina P. Landsberg,^{1,3} Reza Farhadifar,^{2,3} Jonas Ranft,^{2,3} Daiki Umetsu,^{1,3} Thomas J. Widmann,¹ Thomas Bittig,² Amani Said,¹ Frank Jülicher,^{2,*} and Christian Dahmann^{1,*}

¹Max Planck Institute of Molecular Cell Biology and Genetics, Pfotenstrasse 108, 01307 Dresden, Germany

²Max Planck Institute for the Physics of Complex Systems, Nöthnitzer Strasse 38, 01187 Dresden, Germany

Summary

Subdividing proliferating tissues into compartments is an evolutionarily conserved strategy of animal development [1–6]. Signals across boundaries between compartments can result in local expression of secreted proteins organizing growth and patterning of tissues [1–6]. Sharp and straight interfaces between compartments are crucial for stabilizing the position of such organizers and therefore for precise implementation of body plans. Maintaining boundaries in proliferating tissues requires mechanisms to counteract cell rearrangements caused by cell division; however, the nature of such mechanisms remains unclear. Here we quantitatively analyzed cell morphology and the response to the laser ablation of cell bonds in the vicinity of the anteroposterior compartment boundary in developing *Drosophila* wings. We found that mechanical tension is approximately 2.5-fold increased on cell bonds along this compartment boundary as compared to the remaining tissue. Cell bond tension is decreased in the presence of Y-27632 [7], an inhibitor of Rho-kinase whose main effector is Myosin II [8]. Simulations using a vertex model [9] demonstrate that a 2.5-fold increase in local cell bond tension suffices to guide the rearrangement of cells after cell division to maintain compartment boundaries. Our results provide a physical mechanism in which the local increase in Myosin II-dependent cell bond tension directs cell sorting at compartment boundaries.

Results and Discussion

A long-standing hypothesis to explain the maintenance of compartment boundaries is based on differential cell adhesion (or cell affinity [10]). Cell adhesion molecules required for the maintenance of compartment boundaries, however, have not been identified. More recently, it has been proposed that actin-myosin-based tension is important for keeping the dorsoventral compartment boundary of the developing *Drosophila* wing smooth and straight [11, 12]. However, whether a similar mechanism operates at the anteroposterior compartment boundary (A/P boundary) is unclear. Moreover, a physical measurement of differential mechanical tension at compartment boundaries has not been reported. Furthermore, whether and how differential mechanical tension governs cell sorting at compartment boundaries is not well understood.

To test whether actin-myosin-based tension is increased at the A/P boundary (see Figure S1 available online), we quantified the levels of Filamentous (F)-actin and nonmuscle Myosin II (Myosin II). The A/P boundary in the wing disc epithelium was particularly well defined by the cell bonds located at the level of adherens junctions (Figure S2), indicating that mechanisms maintaining the boundary operate at this cellular level. We found that F-actin and the regulatory light chain of Myosin II (encoded by *spaghetti squash*, *sqh*) were increased at these cell bonds along the A/P boundary [11, 12] (Figures S3A–S3D). Cell bonds displaying elevated levels of Myosin II correlate with decreased levels of Par3 (Bazooka in *Drosophila*), a protein organizing cortical domains [13], at the dorsoventral compartment boundary and during germ-band extension in *Drosophila* embryos [11, 12, 14]. Likewise, Bazooka was decreased at cell bonds along the A/P boundary (Figures S3E and S3F), indicating a common mechanism of complementary protein distribution of Myosin II and Bazooka. The level of E-cadherin, a component of adherens junctions, was not altered along the A/P boundary (Figures S3G and S3H).

To identify signatures of increased tension in the vicinity of the A/P boundary, we quantitatively analyzed the morphology of cells at the level of adherens junctions. Line tension and mechanical properties of cells have been proposed to contribute to cell shape and to influence angles between cell bonds [9, 15]. Line tension associated with adherens junctions, here termed cell bond tension, can be defined as the work, per unit length, performed as a cell bond changes its length. Cell bond tension results from actin-myosin bundles and other structural components at junctional contacts that generate tensile stresses. Wing discs from late-third-instar larvae were stained for E-cadherin and *engrailed-lacZ*, a marker for the posterior compartment [16]. Cell bonds were identified, and morphological parameters were analyzed [9] (Figures 1A and 1B). Adjacent anterior and posterior cells (A1 and P1, respectively) displayed a significantly enlarged apical cross-section area compared to cells farther away from the compartment boundary (Figure 1C, Figure S4, and Tables S1 and S2), indicating that apposition of anterior and posterior cells alters specifically the properties of A1 and P1 cells. Angles between adjacent cell bonds along the A/P boundary were larger compared to angles between bonds of the remaining cells (Figure 1D) and were significantly smaller in mutants for Myosin II heavy chain (encoded by *zipper*; *zip²/zip^{Eb}*) (Figure 1D). Thus, the unique morphology of A1 and P1 cells depends on Myosin II. These data are consistent with an increased Myosin II-based tension of cell bonds located along the A/P boundary.

Cells on opposite sides of the A/P boundary differ in gene expression [17]. The homeodomain-containing proteins Engrailed and Invected as well as the Hedgehog ligand are only expressed on the posterior side. The Hedgehog signal is transduced exclusively on the anterior side. Hedgehog signal transduction and the presence of Engrailed and Invected are required to maintain this compartment boundary [18–21]. We tested whether the altered cell morphology at the A/P boundary could be reproduced by ectopically juxtaposing Hedgehog signaling and non-Hedgehog signaling cells.

*Correspondence: julicher@pks.mpg.de (F.J.), dahmann@mpi-cbg.de (C.D.)

³These authors contributed equally to this work

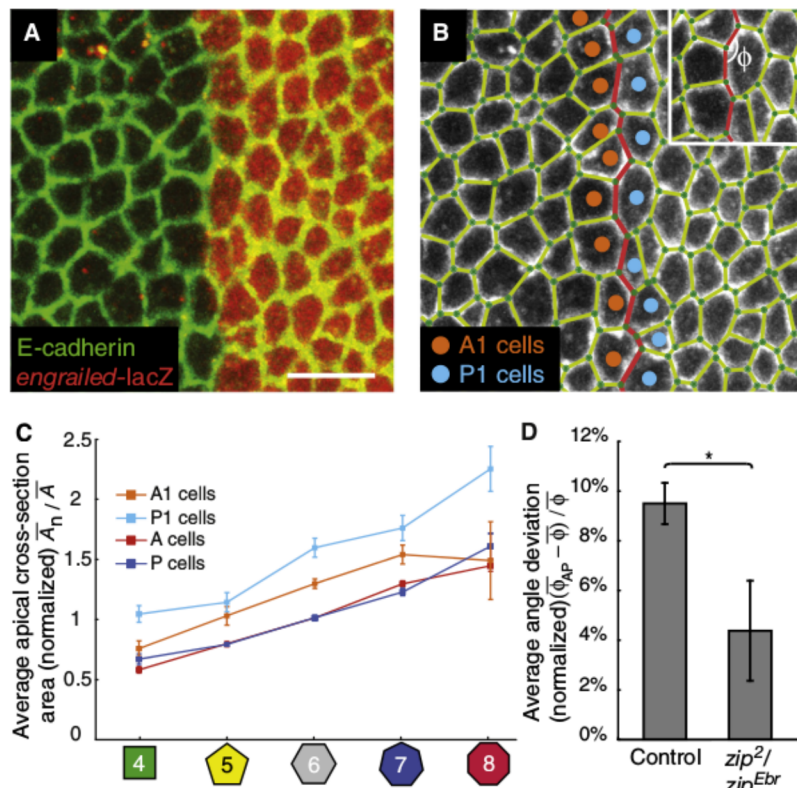


Figure 1. Morphology of Cells at the A/P Boundary
(A) Top view of a control wing disc stained as indicated. The scale bar represents 5 μ m. Anterior is to the left.

(B) Network of cell bonds (light green lines) connected at vertices (green dots) determined by automated image analysis from the image shown in (A). Rows of A1 and P1 cells adjacent to the compartment boundary (red line) and angles $\phi \leq 180^\circ$ between neighboring cell bonds are indicated.

(C) Average apical cross-section areas \bar{A}_n of n-sided cells (polygons), normalized to the average apical cross-section area \bar{A} of each image shown for A1 cells, P1 cells, and all anterior (A) and posterior (P) cells as a function of n. Mean and standard error of the mean (SEM) are shown ($n = 10$ wing discs).

(D) Difference of the average angle $\bar{\phi}_{AP}$ along the A/P boundary and the average angle $\bar{\phi}$ of neighboring bonds within the tissue. Data are averaged over ten images and normalized to $\bar{\phi}$ for control ($zip^{Ebr}/+$) and zip^{Ebr}/zip^2 mutant wing discs. Mean and SEM are shown. (Control: $n_{AP} = 228$, $n = 12429$ from ten wing discs, $\bar{\phi} = 119.80 \pm 0.19^\circ$, for $\bar{\phi}_{AP}$ and $\bar{\phi}$ $p < 0.001$; mutant: $n_{AP} = 114$, $n = 4552$ from ten wing discs, $\bar{\phi} = 119.46 \pm 0.40^\circ$; * $p = 0.007$.)

Clones of cells that expressed Hedgehog from a transgene and that were also mutant for the gene *smoothened* (encoding an essential transducer of the Hedgehog pathway [22, 23]) were generated. In the P compartment, which is refractory to Hedgehog signal transduction, clones displayed a normal morphology (Figures 2A, 2D, and 2G, Table S3). In the A compartment, a response to Hedgehog that is secreted by the clones is elicited in the surrounding wild-type cells. These clones had a rounder appearance ([19] and Figure 2B), and at the clone border, but not away from it, apical cross-section area and bond angles were increased (Figures 2B, 2E, and 2G, Table S4). Similarly, juxtaposing cells expressing *engrailed* and *inverted* with cells that are mutant for these genes resulted in increased apical cross-section area and increased bond angles at the clone border (Figures 2C, 2F, and 2G, Table S5). We conclude that the morphology that is characteristic of cells at the A/P boundary can be imposed on cells within a compartment by juxtaposing cells with different activities of Hedgehog signal transduction or Engrailed and Inverted.

Ablating cell bonds generates cell vertex displacements, providing direct evidence for tension on cell bonds [24]. We ablated individual cell bonds by using a UV laser beam focused in the plane of the adherens junctions [9]. Single-cell bonds were cut, and the displacement of vertices of neighboring cells, visualized by E-cadherin-GFP, was recorded. The P compartment was visualized by expression of GFP-gpi under control of the *engrailed* gene via the GAL4/UAS system. The increase in distance between the two vertices of the ablated cell bond and the initial velocity of this vertex separation were analyzed (see Supplemental Experimental Procedures, Figures S5A–S5F). The ratio of initial velocities in response to cell bond ablation is a measure of the tension ratio on these cell bonds [25]. Initial velocity and extent of vertex separation were indistinguishable between anterior (A/A) and posterior

(P/P) cell bonds located away from the A/P boundary (Figures 3A–3C, Table S6, Movies S1 and S2). This was also the case when specifically cell bonds between the first and second row of anterior cells were ablated (Figures 3B and 3C, Movie S3). By contrast, ablation of bonds between adjacent anterior

and posterior cells (A/P cell bonds) gave rise to a larger vertex separation (Figures 3A and 3B, Movie S4). This result was not due to the fact that A/P cell bonds have a preferred orientation (Figure S5G). Moreover, the initial velocity of ablated A/P bonds was 2.37 ± 0.38 (mean and standard error)-fold higher compared to the mean of initial velocities of A/A and P/P bonds (Figure 3C, Table S6). This value provides an estimate of the ratio λ of cell bond tension along the A/P boundary relative to the average tension of cell bonds. In the presence of the Rho-kinase inhibitor Y-27632 [7], the ratio of initial velocity of vertex separation of A/P cell bonds relative to A/A cell bonds was reduced to 1.46 ± 0.28 (Figure 3C, Movies 5 and 6, Table S6). Given that Myosin II is the main effector of Rho-kinase [8], these results strongly suggest that Myosin II-based tension acting on cell bonds is locally increased along the A/P boundary.

To quantify λ by an independent method, we calculated the displacement field after laser ablation (Figures 3D–3F). Using our vertex model ([9]; see Box 1), we introduced two populations of adjacent cells and simulated cell bond ablations, varying λ between 1 and 4. When $\lambda = 2.5$, the vertex displacement, and in particular the anisotropy of displacements, in the simulations closely matched the vertex displacements in the experiment (Figures 3G–3I). In the vertex model, $\lambda = 2.5$ also resulted in increased bond angles at the interface of the two cell groups (Figures S6A and S6B), similar to the A/P boundary in the wing disc. Thus, on the basis of two different methods, our data demonstrate that cell bond tension is increased approximately 2.5-fold along the A/P boundary compared to the remaining tissue.

To test whether a 2.5-fold increase in cell bond tension is sufficient to maintain a compartment boundary, we used our vertex model to simulate the growth of two adjacent cell populations for $\lambda = 1$, 2.5, and 4. For $\lambda = 1$, the interface between

Box 1. Description of a Network of Adherens Junctions by a Vertex Model

In the vertex model, the network of adherens junctions is described by polygons characterized by the vertex positions R_i were the index i numbers the vertices [9]. Stable configurations are local minima of a work function

$$E(R_i) = \sum_{\alpha} \frac{K}{2} A_{\alpha} - A_{\alpha}^{(0)} + \sum_{\langle ij \rangle} \Delta_{ij} + \sum_{\alpha} \frac{\Gamma}{2} L_{\alpha}^2;$$

The first term describes area elasticity of cells indexed by α , with area A_{α} , preferred area $A_{\alpha}^{(0)}$, and elastic coefficient K . The second term describes the effects of tension Δ_{ij} along a cell bond $\langle i, j \rangle$ of length l_{ij} that connects vertices i and j . The last term describes the elasticity of cell perimeter L_{α} by the coefficient Γ . The cell bond tension Δ_{ij} and the coefficient Γ describe the line tension at adherens junctions and depend on actin-myosin contractility and cell-cell adhesion. We introduced an interface (red line) between anterior and posterior cell populations. For all cells, except A1 cells and P1 cells, $A_{\alpha}^{(0)} = A^{(0)}$ and for all bonds, except along the interface, $\Delta_{ij} = \Delta$ are equal. For A1 cells and P1 cells,

$A_{\alpha}^{(0)} = 1:1 A^{(0)}$ to mimic the observed increase in cross-section area of A1 and P1 cells. The tension of bonds along the interface is increased by a factor λ : $\Delta_{ij} = \lambda \Delta$.

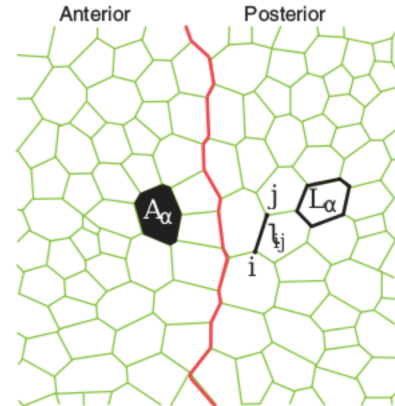


Figure A. Network of Adherens Junctions

two growing cell populations became increasingly irregular (Figure 4A, Movie S7). By contrast, for $\lambda = 2.5$ and 4, a well-defined interface was maintained (Figure 4B, Movies S8 and

S9). Moreover, corresponding changes in cell bond tension at borders of simulated clones resulted in the morphology and sorting behavior of cell patches that resembled those

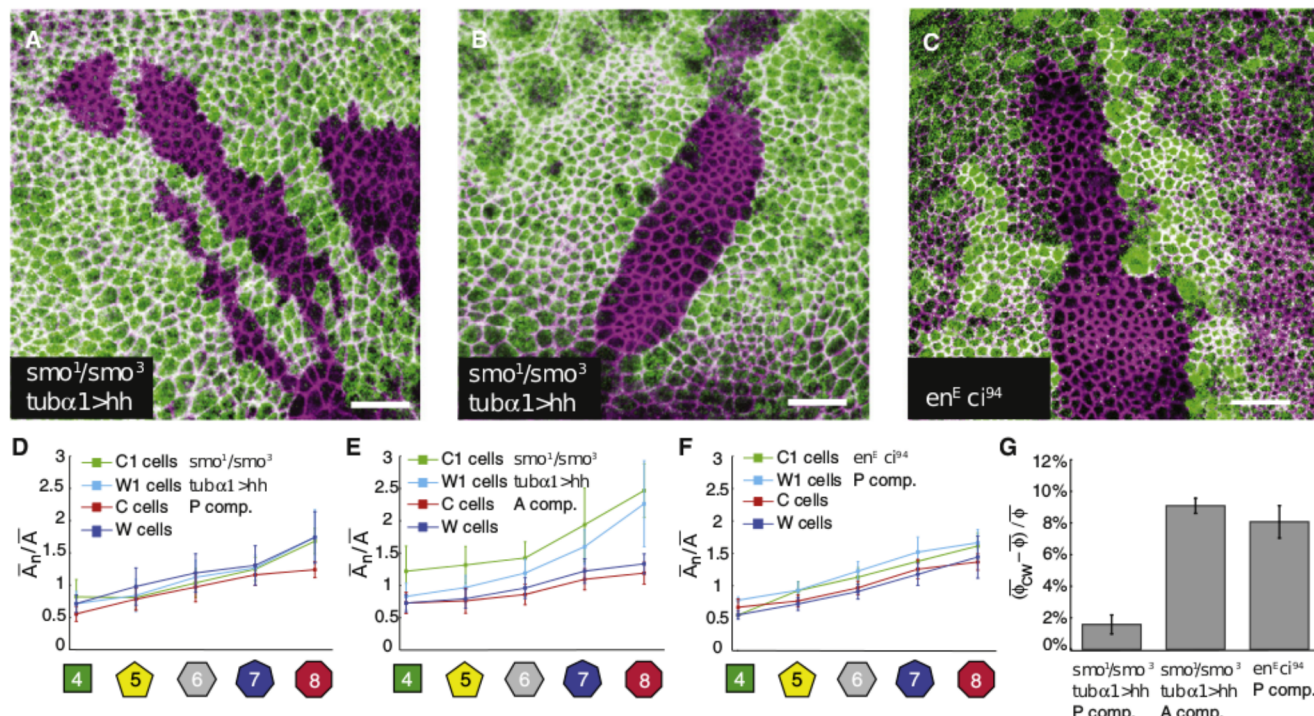


Figure 2. Morphology of Cells at Ectopic Borders of Hedgehog Signal Transduction or Engrailed and Invected Activity
(A–C) *smo¹/smo³, tub α 1>hh* (A and B) or *en^E ci⁹⁴* (C) clones of cells located in the (A and C) posterior or (B) anterior compartment identified by the absence of (A and B) CD2 or (C) GFP staining (green). E-cadherin staining is shown in magenta.

(D–F) Average apical cross-section areas of n-sided cells \bar{A}_n , normalized to the average apical cross-section area \bar{A} of each image shown for clone cells C1 and wild-type cells W1, adjacent to the interface between the clone cells (C cells) and wild-type cells (W cells), and for C and W cells. Data shown in (D), (E), and (F) correspond to the experiments depicted in (A), (B), and (C), respectively. Mean and SEM are shown.

(G) Difference of the average angle ϕ_{CW} along the clone boundaries and the average angle in the entire image $\bar{\phi}$ normalized to $\bar{\phi}$ for the experiments shown in (A)–(C). Mean and SEM are shown ($p = 0.027$, $p < 0.001$, and $p < 0.001$, $n = 228, 240$, and 332 angles at clone borders and $2960, 9979$, and 7441 for angles elsewhere in the images for experiments depicted in A, B, and C, respectively).

Scale bars represent 10 μ m.

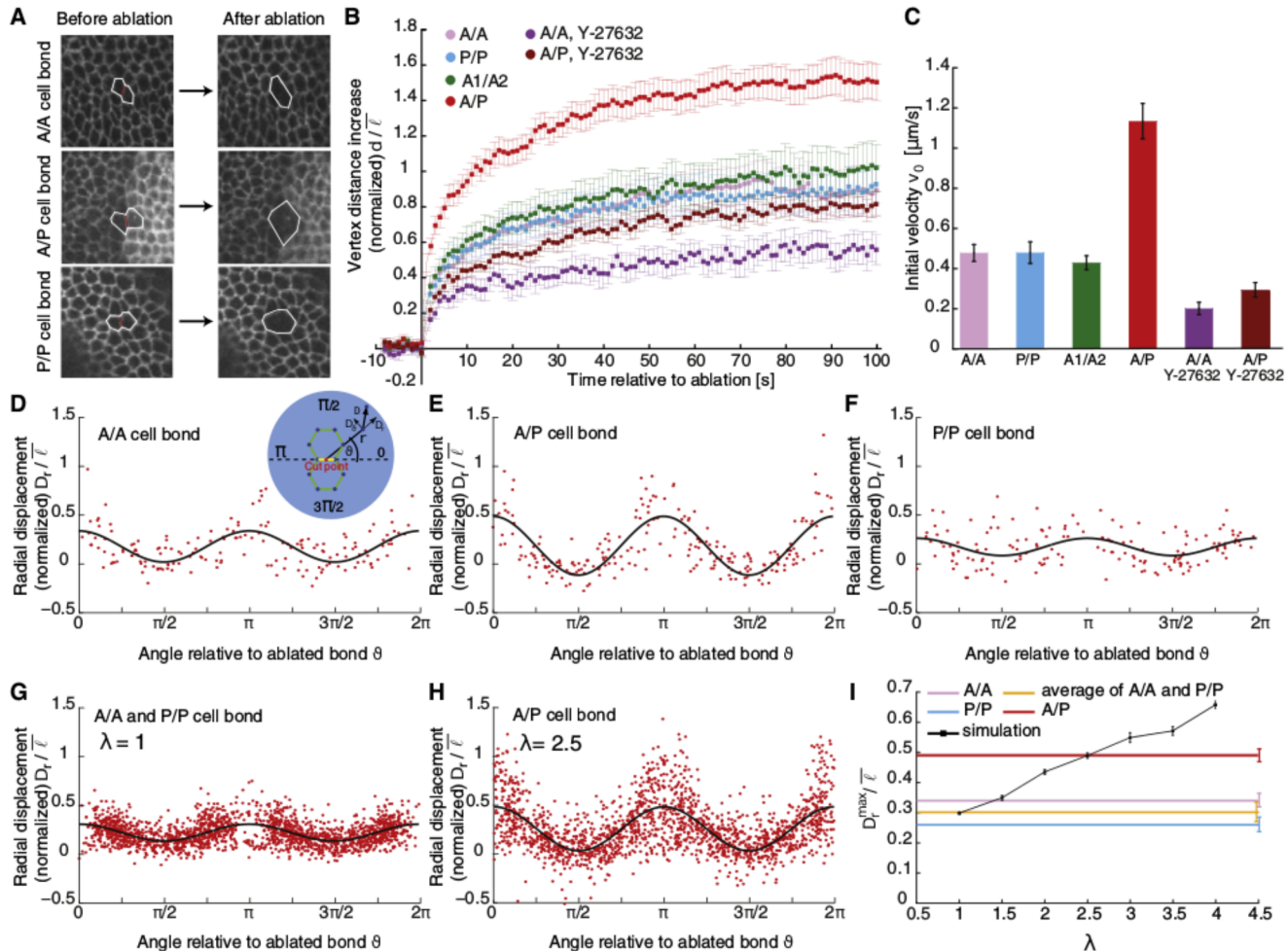


Figure 3. Vertex Displacements in Response to Laser Ablation of Cell Bonds

(A) Images of E-Cadherin-GFP-expressing wing discs before and after single-cell bonds were ablated. Posterior cells are also labeled by GFP-gpi. (B) Change in distance d between vertices at the ends of cell bonds after ablation as a function of time. Values are normalized to the average cell bond length $\bar{\ell} = 1.7 \mu\text{m}$. The types of ablated cell bonds are indicated. A₁/A₂ refers to cell bonds between A₁ cells and their anterior cell neighbors. Mean and SEM are shown. (C) Initial velocity v_0 of vertex separation shown in (B). Mean and standard error are shown. (D–F) Patterns of radial displacement D_r of all vertices located at a distance of up to two average bond lengths from the cut point (red dots) shown as a function of the angle θ (see inset in D). Values are normalized to the average bond length $\bar{\ell}$. A fit of the data points to a cosine function is shown (black line). Inset in (D) is a schematic representation of displacement vectors D with radial component D_r and tangential component D_θ of vertices located at distance r from the cut point (red dot) at an angle θ relative to the cut bond axis (yellow line). The number of experiments was as follows: A/A, $n = 20$; P/P, $n = 17$; and A/P, $n = 26$. (G and H) Same as (D)–(F), except that data were obtained by simulating A/A and P/P cell bond ablations for $\lambda = 1$ (G) and A/P cell bond ablations for $\lambda = 2.5$ (H). (I) Maxima of the radial displacements D_r^{\max} determined by the fits shown in (D)–(H) normalized to the average cell bond length $\bar{\ell}$. The mean experimental values are indicated as horizontal lines (standard errors are depicted). The mean values and standard errors obtained from simulations with different λ are shown as black squares and bars.

of experimental cell clones compromised for Hedgehog signal transduction or Engrailed and Invected activity (Figures S6C–S6F, see [Supplemental Experimental Procedures](#)). The roughness of the interface (see [Supplemental Experimental Procedures](#), Figure S7) in our simulations decreased with increasing λ (Figure 4C), showing that cell bond tension is sufficient to maintain straight interfaces between growing cell populations. For $\lambda = 2.5$, the roughness of the interface was still larger than the roughness of the A/P boundary in wing discs (Figure 4C). This suggests that additional mechanisms might contribute to further reduce the roughness of the A/P boundary. Also, because of the uncertainty of the

mechanical properties of A₁ and P₁ cells, which differ from those of the remaining cells, the value of λ , inferred from laser ablation of cell bonds, might be underestimated. Remarkably, the roughness of the A/P boundary could be altered in mutant conditions. In *zip²/zip^{Ebr}* mutant wing discs, the roughness of the compartment boundary was significantly larger than in controls (Figure 4C, Figure S8), demonstrating a role for Myosin II in maintaining a sharp and straight A/P boundary.

In summary, by applying physical approaches and quantitative imaging, our work for the first time demonstrates and quantifies an increase in tension confined to the cell bonds

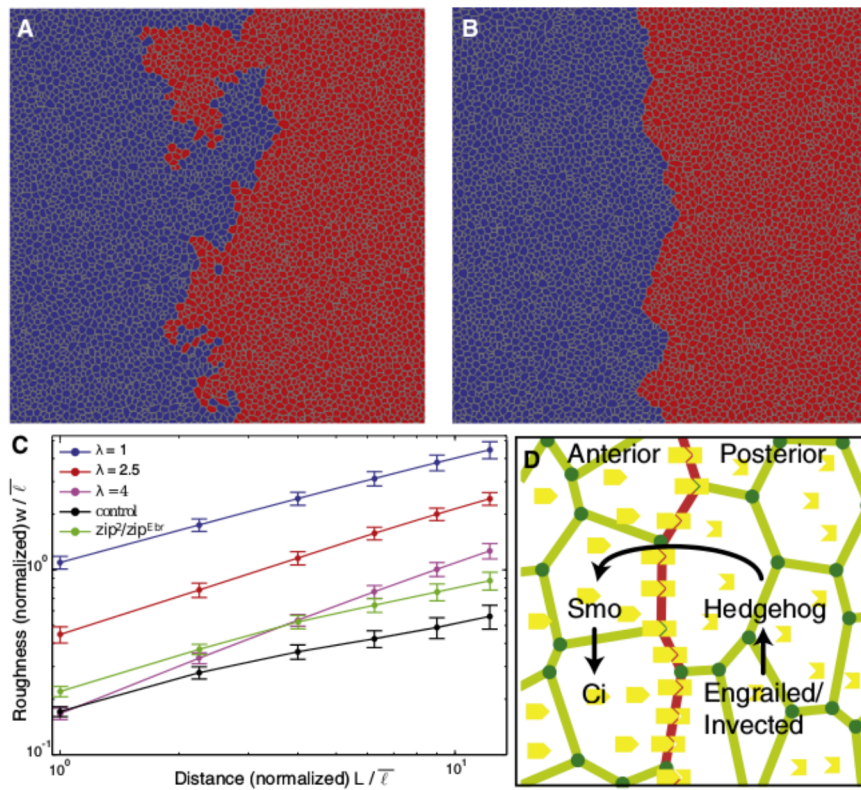


Figure 4. Simulations of Interfaces between Two Growing Cell Populations

(A and B) Final configurations of the networks of cell bonds obtained by simulating the growth of two adjacent cell populations (anterior is blue and posterior is red) for values of (A) $\lambda = 1$ and (B) $\lambda = 2.5$. (C) Roughness w of the interface between two cell populations as a function of distance L parallel to the interface normalized by the average bond length ℓ for simulations with different values of λ as indicated and for the A/P boundary in control ($zip^{Ebr}/+$) and zip^2/zip^{Ebr} mutant third-instar wing discs. Mean and SEM are shown (for control and zip^2/zip^{Ebr} : $p = 0.02$ – 0.04 for different L , $n = 5$). (D) Model of heterotypic interactions between two gene products (yellow pentagons) at the A/P boundary (red line) guiding cell sorting and a simplified view of the Hedgehog signaling system (see legend to Figure S1).

Supplemental Data

Supplemental Data include nine figures, six tables, Supplemental Experimental Procedures, and ten movies and can be found with this article online at [http://www.cell.com/current-biology/supplemental/S0960-9822\(09\)01840-5](http://www.cell.com/current-biology/supplemental/S0960-9822(09)01840-5).

Acknowledgments

We are grateful to H. Bringmann, S. Grill, A. Hyman, M. Mayer, and J.-C. Röper for providing us with the laser-ablation system and for assisting us in its use. We thank K. Basler, S. Eaton, and K. Irvine for fly stocks, E. Knust and the Developmental Studies Hybridoma Bank for antibodies, M. Aliee for help with determining the roughness of interfaces, C. Schuster for help with live imaging of dividing cells, and J. Howard and E. Knust for critical comments on the manuscript. This work was supported by the Max Planck Society, by an EMBO Long-Term Fellowship (D.U.), and by a grant from the Deutsche Forschungsgemeinschaft (C.D.).

along the A/P boundary. Moreover, simulations show that this increase in tension suffices to maintain a stable interface between two proliferating cell populations. Genetic studies demonstrated that cells of the two compartments differ in their expression profiles and signaling activities [17]. It has therefore been proposed that biophysical properties of cells within the P compartment differ from those within the A compartment, and that such differences could drive cell sorting [18, 19, 21, 26, 27]. When quantifying cell morphology and vertex displacements after laser ablation, we detected no differences in the biophysical properties of cells between the two compartments. However, the two rows of abutting A and P cells show clear differences in biophysical properties from other cells. Most importantly, the cell bond tension along the A/P boundary is increased. Cell divisions in the vicinity of the A/P boundary were randomly oriented in the epithelial plane (Figure S9, Movie S10). Thus, taken together with our simulations, our results suggest a sorting mechanism by which an increased cell bond tension guides the rearrangement of cells after cell division to maintain a straight interface. Increased cell bond tension and the roughness of the A/P boundary depend on Rho kinase activity and Myosin II, indicating a role for actin-myosin-based tension in this process. Because cell bond tension also depends on cell-cell adhesion, differences in the adhesion between A1 and P1 cells as compared to the remaining cells might also contribute to sorting. The heterotypic, but not homotypic, interaction of molecules presented on the surface of A and P cells might trigger the local increase in cell bond tension. Hedgehog signal transduction and the presence of Engrailed and Invected might control the expression of these heterotypically interacting molecules (Figure 4D). Our data indicate an important role for cell bond tension directing cell sorting during animal development.

Received: March 18, 2009
Revised: October 1, 2009
Accepted: October 2, 2009
Published online: October 29, 2009

References

- Blair, S.S. (2003). Lineage compartments in *Drosophila*. *Curr. Biol.* **13**, R548–R551.
- Dahmann, C., and Basler, K. (1999). Compartment boundaries: At the edge of development. *Trends Genet.* **15**, 320–326.
- Irvine, K.D., and Rauskolb, C. (2001). Boundaries in development: Formation and function. *Annu. Rev. Cell Dev. Biol.* **17**, 189–214.
- McNeill, H. (2000). Sticking together and sorting things out: Adhesion as a force in development. *Nat. Rev. Genet.* **1**, 100–108.
- Teppas, U., Godt, D., and Winklbauer, R. (2002). Cell sorting in animal development: Signalling and adhesive mechanisms in the formation of tissue boundaries. *Curr. Opin. Genet. Dev.* **12**, 572–582.
- Vincent, J.P. (1998). Compartment boundaries: Where, why and how? *Int. J. Dev. Biol.* **42**, 311–315.
- Uehata, M., Ishizaki, T., Satoh, H., Ono, T., Kawahara, T., Morishita, T., Tamakawa, H., Yamagami, K., Inui, J., Maekawa, M., et al. (1997). Calcium sensitization of smooth muscle mediated by a Rho-associated protein kinase in hypertension. *Nature* **389**, 990–994.
- Winter, C.G., Wang, B., Ballew, A., Royou, A., Karess, R., Axelrod, J.D., and Luo, L. (2001). *Drosophila* Rho-associated kinase (Drok) links Frizzled-mediated planar cell polarity signaling to the actin cytoskeleton. *Cell* **105**, 81–91.
- Farhadifar, R., Roper, J.C., Aigouy, B., Eaton, S., and Julicher, F. (2007). The influence of cell mechanics, cell-cell interactions, and proliferation on epithelial packing. *Curr. Biol.* **17**, 2095–2104.

10. Garcia-Bellido, A. (1975). Genetic control of wing disc development in *Drosophila*. *Ciba Found. Symp.* 0, 161–182.
11. Major, R.J., and Irvine, K.D. (2005). Influence of Notch on dorsoventral compartmentalization and actin organization in the *Drosophila* wing. *Development* 132, 3823–3833.
12. Major, R.J., and Irvine, K.D. (2006). Localization and requirement for Myosin II at the dorsal-ventral compartment boundary of the *Drosophila* wing. *Dev. Dyn.* 235, 3051–3058.
13. Knust, E., and Bossinger, O. (2002). Composition and formation of inter-cellular junctions in epithelial cells. *Science* 298, 1955–1959.
14. Blankenship, J.T., Backovic, S.T., Sanny, J.S., Weitz, O., and Zallen, J.A. (2006). Multicellular rosette formation links planar cell polarity to tissue morphogenesis. *Dev. Cell* 11, 459–470.
15. Brodland, G.W., and Chen, H.H. (2000). The mechanics of heterotypic cell aggregates: Insights from computer simulations. *J. Biomech. Eng.* 122, 402–407.
16. Hama, C., Ali, Z., and Kornberg, T.B. (1990). Region-specific recombination and expression are directed by portions of the *Drosophila engrailed* promoter. *Genes Dev.* 4, 1079–1093.
17. Lawrence, P.A., and Struhl, G. (1996). Morphogens, compartments, and pattern: Lessons from *Drosophila*? *Cell* 85, 951–961.
18. Blair, S.S., and Ralston, A. (1997). Smoothened-mediated Hedgehog signalling is required for the maintenance of the anterior-posterior lineage restriction in the developing wing of *Drosophila*. *Development* 124, 4053–4063.
19. Dahmann, C., and Basler, K. (2000). Opposing transcriptional outputs of Hedgehog signalling and engrailed control compartmental cell sorting at the *Drosophila* A/P boundary. *Cell* 100, 411–422.
20. Morata, G., and Lawrence, P.A. (1975). Control of compartment development by the *engrailed* gene in *Drosophila*. *Nature* 255, 614–617.
21. Rodriguez, I., and Basler, K. (1997). Control of compartmental affinity boundaries by hedgehog. *Nature* 389, 614–618.
22. Alcedo, J., Ayzenzon, M., Von Ohlen, T., Noll, M., and Hooper, J.E. (1996). The *Drosophila smoothened* gene encodes a seven-pass membrane protein, a putative receptor for the Hedgehog signal. *Cell* 86, 221–232.
23. van den Heuvel, M., and Ingham, P.W. (1996). *smoothened* encodes a receptor-like serpentine protein required for Hedgehog signalling. *Nature* 382, 547–551.
24. Kiehart, D.P., Galbraith, C.G., Edwards, K.A., Rickoll, W.L., and Montague, R.A. (2000). Multiple forces contribute to cell sheet morphogenesis for dorsal closure in *Drosophila*. *J. Cell Biol.* 149, 471–490.
25. Rauzi, M., Verant, P., Lecuit, T., and Lenne, P.F. (2008). Nature and anisotropy of cortical forces orienting *Drosophila* tissue morphogenesis. *Nat. Cell Biol.* 10, 1401–1410.
26. Steinberg, M.S. (1963). Reconstruction of tissues by dissociated cells. Some morphogenetic tissue movements and the sorting out of embryonic cells may have a common explanation. *Science* 141, 401–408.
27. Garcia-Bellido, A., Ripoll, P., and Morata, G. (1973). Developmental compartmentalisation of the wing disk of *Drosophila*. *Nat. New Biol.* 245, 251–253.